PAPER

Demonstration of Biofouling Mitigation Methods for Long-Term Deployments of Optical Cameras

AUTHORS

James Joslin
Brian Polagye
Northwest National Marine Renewable Energy Center, University of Washington

ABSTRACT

Biofouling mitigation measures for optical ports can extend the duration of oceanographic deployments, but there have been few quantitative studies of field performance. Results are presented from a 4-month field test of a stereo-optical camera system intended for long-term environmental monitoring of tidal turbines. A combination of passive (copper rings and ClearSignal antifouling coating) and active (mechanical wipers) biofouling mitigation measures are implemented on the optical ports of the two cameras and four strobe illuminators. Biofouling on the optical ports is monitored qualitatively by periodic diver inspections and quantitatively by metrics describing the quality of the images captured by cameras with different antifouling treatments. During deployment, barnacles colonized almost every surface of the camera system, except the optical ports with fouling mitigation measures. The effectiveness of the biofouling mitigation measures suggests that 4-month deployment durations are possible, even during conditions that would otherwise lead to severe fouling and occlusion of optical ports.

Keywords: biofouling, optical cameras, environmental and remote monitoring, field testing

Introduction

Biofouling is often a limiting factor for long-term deployments of oceanographic optical instrumentation. While this study focuses on the fouling of camera optical ports, the methods and outcomes may be relevant to other instruments that rely on light transmission, such as absorption-attenuation meters (AC meters), photosynthetically active radiation (PAR) sensors, or fluorometers (Manov et al., 2004). The sensitivity of each optical sensor to biofouling can vary greatly, and results from one instrument should not be extrapolated to another. As biological growth colonizes a camera's optical port, image quality degrades, and the monitoring mission may be compromised. With the proliferation of cabled ocean observatories (Chave et al., 2009; Howe & McGinnis, 2004; Woodroffe et al., 2008), long-term deployments of optical instrumentation are becoming more common, and biofouling mitigation methods are receiving more attention. Research in this field is generally focused on improving understanding of fundamental biofouling mechanisms (such as adhesion and growth) (Phang et al., 2007; Salta et al., 2013) or development of biofouling mitigation measures. For example, Manov et al. (2004) discuss the use of copper to prolong deployments of open, enclosed, or semi-enclosed and shuttered optical instrumentation, and Debiemme-Chouvy et al. (2011) describe applications of electrochemisty to produce a biocide on the optical port surface. Whelan and Regan (2006) and Delauney et al. (2010) provide reviews of existing biofouling mitigation techniques and their implementation on different sensors.

Marine renewable energy, including wave, tidal and ocean current, and offshore wind energy, is a growing sector of the electricity generation industry that requires robust approaches to biofouling. Energy converters and their support structures are deployed in the marine environment for multi-year periods and cannot expect to receive significant maintenance if their cost of energy is to be competitive with conventional forms of electricity generation. While biofouling is possible on any of the converter surfaces, general-purpose biofouling mitigation methods may be different from the approach taken for more sensitive components, such as sensor transducers. Optical camera observations have been proposed to inform a number of critical environmental questions (Polagye et al., 2014), and the shore cables for the energy converters provide sufficient power and data bandwidth to support high-resolution optical measurements over extended

periods. This paper discusses the implementation of biofouling mitigation measures on the optical ports of a camera system developed for long-term monitoring of marine energy converters (Joslin et al., 2014a). This system will be recovered periodically for maintenance (Joslin et al., 2013), and it is expected that optical port fouling will be the limiting factor for the interval between maintenance. Methods to quantitatively evaluate the effectiveness of these biofouling mitigation measures are developed and applied to a multi-month endurance test of the camera system.

Methodology

Field Deployment Configuration

Figure 1 illustrates the stereo-optical camera system developed for monitoring marine renewable energy converters (Joslin et al., 2014a). The integrated system combines two Allied Vision Technologies Manta G-201 machine vision optical cameras, four Excelitas Technologies MVS-5000 strobes, and the supporting power and communications infrastructure to cable the system to a shore station. The system is controlled in real time by a computer on shore that can adjust camera settings (e.g., frame rate, exposure time, digital gain, and strobe triggering) and archive acquired stereo imagery. The optical cameras and strobes are marinized by enclosing them in aluminum pressure housings with planar acrylic optical ports. Material selection has been shown to influence the rate of biofouling on optical ports (Manov et al., 2004), and although not optimal for biofouling, abrasion resistant acrylic is used here due to its transparency for optical imagery and ease of manufacturing for integration in the pressure housings.

A multi-month field trial was conducted during early 2013 to evaluate overall system endurance (hardware performance, software stability, corrosion, and biofouling). After an initial calibration in a tank, the system was deployed from January 24 to February 8 in freshwater off of a dock on Lake Union, WA. Subsequently, the system was deployed in a saltwater environment from March 3 to July 2 off Edmonds, WA.

For the salt-water endurance trial, the camera system was mounted to the test frame shown in Figure 2. The Applied Physics Laboratory vessel *R/V Jack Robertson* lowered the test frame to the seabed in approximately 20 m of water at a point 100 m from shore. Mounted to this frame, the camera system was suspended 5 m above the seabed in a downward-looking orientation. The power and fiber umbilical was terminated on shore and connected to a data logging computer. Divers from the Applied Physics

FIGURE 1

Prototype imaging system showing principal components and scale.

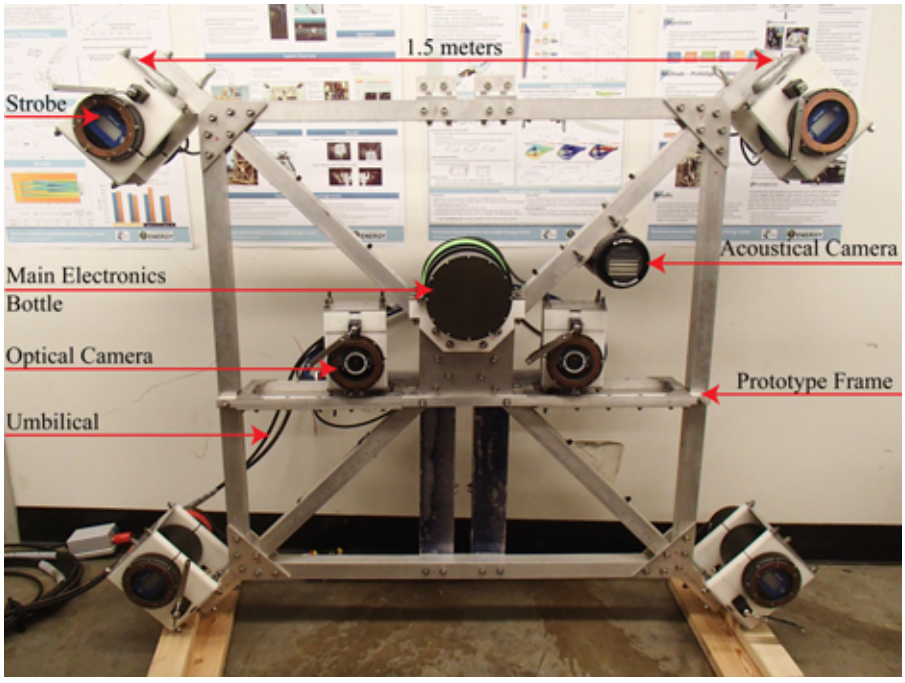

FIGURE 2

Five-meter-tall field test frame on the deck of the deployment vessel *R/V Jack Robertson*.

Laboratory at the University of Washington visually inspected the system for biofouling and corrosion on March 3, April 11, May 3, and June 26.

Biofouling Mitigation Measures

A combination of active and passive biofouling mitigation measures are implemented on the optical ports of the two cameras and four strobe housings. As shown in Figure 3, each 4-inch optical port has a ring of copper (Cu) around its perimeter, which is intended to suppress biofouling at the edge of the optical port. Each housing is also equipped with a mechanical brush wiper (Wi) manufactured by Zebra-Tech Ltd. (http://www.zebra-tech.co.nz/Hydro-Wiper). In addition, each of the camera and strobe ports is coated with the ClearSignal fouling release coating (CS) produced by Severn Marine Technologies (http://www.severnmarinetech.com/). This combination of biofouling mitigation measures is selected based on the demonstrated effectiveness of copper shutters (Manov et al., 2004) and the potential additional benefit of the ClearSignal coating. Interactions between the copper, wiper, and release coating are theorized to increase the antifouling effectiveness over each measure individually. A fully shuttered system was considered but deemed undesirable for optical cameras since failure in the closed position would obviate any data collection and large shutters would be subject to significant structural loads while open in an energetic environment (wave or current). Ultraviolet lights were similarly considered but not implemented due to the uncertainty in the appropriate wavelengths for preventing fouling and limited documentation of this field in the literature (Manov et al., 2004).

The wiper, when triggered by the control computer in the shore station, sweeps a 90° arc across the copper ring and optical port before reversing direction and returning to its "home" position. This action may transfer trace amounts of copper from the ring across the optical port over the course of many wipe cycles, thus increasing the effectiveness of the wiper in isolation. This is, however, a hypothesis that was not part of the test matrix during this field trial (e.g., removing the copper ring from one of the pressure housings with a wiper). Throughout the endurance test, the wipers actuated once per hour during normal system operation. Electrical interference in the serial communication bus between the shore computer and camera system required the system to be shut down on six occasions, during which the wipers were not actuated. For the final month of the deployment, the system did not run continuously because of continued degradation of the communication bus. To continue collecting biofouling data during this period, the cameras were brought on-line manually each night to capture images. For this month, the mechanical wipers on the cameras actuated once every 24 h, and the wipers on the strobes were inactive. During this same period, the mechanical wiper on Camera 2 (Cu and Wi) malfunctioned and would periodically stop in front of the optical port after a wipe cycle, thereby blocking part of the image. This did not affect the wiper's ability to remove fouling but did complicate quantification of biofouling rates (see the following section). This malfunction was caused by a gradual increase in friction between the wiper and the optical port caused by fouling on the wiper brush and may be avoided by decreasing the interference spacing between the wiper brush and port.

Figure 4 illustrates the arrangement of the biofouling mitigation measures on the six optical ports in the system. Strobe 3 (Cu) was intended to serve as a control with minimal antifouling protection by disabling the wiper. However, an interruption to the bottle's power supply would cause

FIGURE 3

Biofouling mitigation measures on an optical camera port (preendurance test).

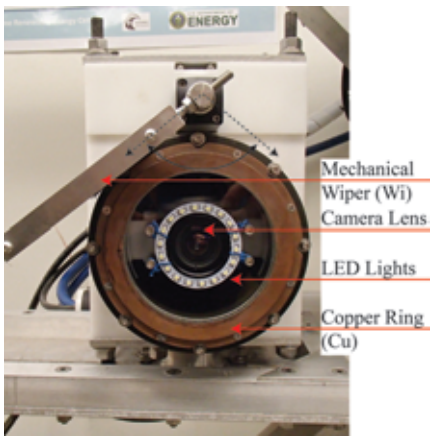

FIGURE 4

Arrangement of antifouling measures on camera system optical ports (*S* denotes strobe, *C* denotes camera, and *MEB* denotes the main electronics bottle).

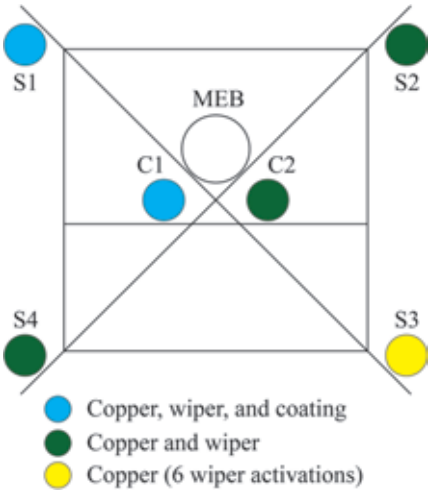

the wiper to automatically actuate, and since the system was power cycled on six occasions, the results for this optical port cannot be considered a control case.

Qualitative and Quantitative Evaluation of Biofouling Mitigation Measures

Performance of biofouling mitigation measures was monitored qualitatively during the endurance trial by diver inspections and quantitatively through the images captured by the cameras. During the inspections, the divers visually checked for the presence or absence of macrofouling on the six optical ports and adjacent surfaces but did not disturb the surfaces or attempt to quantify the degree or type of fouling. More precise methods (ASTM D6990-05, 2011; Dobretsov et al., 2014) to quantify fouling during inspections were not attempted due to diver limitations. A final qualitative assessment of the biofouling on the system and all of the optical ports was conducted post-recovery on July 2.

During testing, the optical cameras collected sequences of 10 images at 10 frames per second once every 15 min to monitor interactions between marine life and the frame (such as fish, crabs, and starfish) and provide some indication of test platform integrity between inspection dives. To monitor the biofouling levels on the camera optical ports, a ring of LED lights is installed within the camera housing, at the perimeter of the camera lens. On an hourly basis, sequences of 10 images were captured with these LEDs backlighting the optical port, as shown in Figure 5. Biofouling on the optical port is illuminated by the LEDs and shows increased brightness relative to clean conditions. This allows the extent and severity of biofouling to be contrasted for the two combinations of mitigation treatments applied to the camera optical ports (Cu, Wi, and CS on Camera 1 versus Cu and Wi on Camera 2).

FIGURE 5

Cross-sectional schematic of camera bottle demonstrating the photon path from LED lights to camera lens as a reflection of biofouling or flocculent.

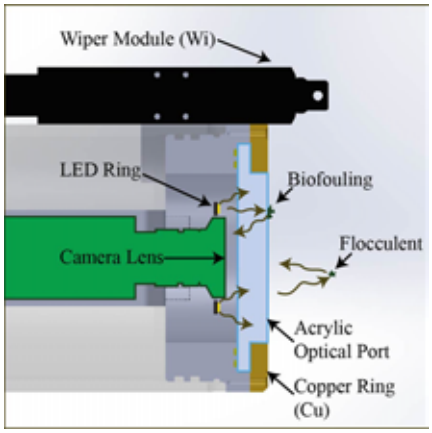

The brightness, B, of an image collected at time t with the LED illumination activated is calculated as a summation of pixel grayscale values, $p(x,y)$, as

$$B(t) = \sum_{x=1}^{n} \sum_{y=1}^{m} p(x,y) \quad (1)$$

For this camera configuration, the image resolution is n = 1624 and m = 1234 with a pixel grayscale range of 0–255.

A time-varying biofouling metric, $F(t)$, for each acquired image is calculated as

$$F(t) = \frac{(B(t) - B(0))}{(B_{\max} - B(0))}. \quad (2)$$

where $B(0)$ is the baseline value corresponding to the brightness levels on the first night of the deployment and $B_{\max}$ is the maximum possible brightness value ($255 \times n \times m$). This metric takes on values between zero (for the baseline images) and unity (for a fully obscured optical port).

Figure 6 demonstrates the effectiveness of this method for quantifying

FIGURE 6

Demonstration images for biofouling metric calculations with LED backlighting. (a)–(c) show representative image quality for (a) a clear optical port with the LEDs inactive, (b) a partially obscured (F = 0.37) optical port, and (c) a fully obscured (F = 1.0) optical port. (d)–(f) show the corresponding image brightness with the LEDs active.

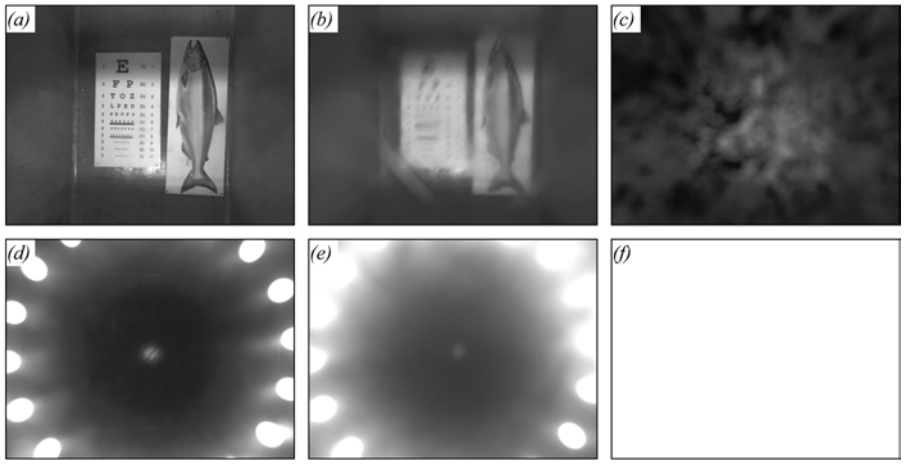

fouling on a camera's optical port by showing the quality of images captured with external illumination alongside images captured with the internal LED backlight for a clear ($F = 0$), blurry ($F = 0.37$), and fully obscured ($F = 1.0$) optical port. The artificial fouling in these images is simulated in the laboratory using a light coating of silicone grease as adhesive and fine sand to obscure the image. The maximum acceptable biofouling metric for optical images depends on the monitoring mission intended for the system. Missions requiring high image resolution (e.g., precise measurements of target size and speed using stereo processing) will have a lower threshold than simpler missions (e.g., fish detection within a few meters of the camera).

The hourly biofouling images were collected in three sets of 10 images with camera exposure times of 10, 25, and 50 ms. This range of exposure times is used to evaluate the method's sensitivity to camera configuration. For all three exposures, images were acquired at a rate of 1 frame per second, no digital gain was used, and the strobes were not triggered. By averaging the sets of 10 images collected each hour, the variations in backscattered light caused by moving flocculent in the water are reduced. A daily mean biofouling metric is calculated as

$$\overline{F(t)} = \sum_{i=1}^{N} F_i(t) \Big/ N \qquad (3)$$

where $F_i(t)$ is the fouling metric for each image and N is the number of images used from each day. Only images collected during nighttime hours ($N = \sim 80$) are used for each camera configuration to avoid the confounding effect of variable external illumination.

Results

Field Deployment

Diving inspections confirmed increasing macrofouling on the test frame throughout the deployment (also observed in camera imagery), while the optical ports were observed to remain clear of fouling until the final (June 26) inspection. During this final inspection, the strobe optical ports (which were no longer being actively wiped) were observed to have varying degrees of macrofouling while the camera ports remained clear. Figure 7 shows the increasing level of biofouling on the test frame from camera images acquired over the course of the deployment.

Biofouling Mitigation Measures

Figure 8 shows the calculated daily mean biofouling metric for each camera from the images collected with 50-ms exposure times throughout the endurance trial. Qualitatively similar trends were observed with 10- and 25-ms exposure settings, suggesting an insensitivity to exposure time. Highlighted periods represent interruptions in system operation due to software errors, electrical interference with serial communications, and wiper malfunctions. As previously discussed, during the last month of the deployment, the system operation was reduced to a short period every night such that the number of images used for the nightly average was reduced to 10 from ~80. On three occasions during this same period, the wiper on Camera 2 (Cu and Wi) malfunctioned and partially obscured the images that were collected, preventing the calculation of a metric for that night.

The biofouling metric values shown in Figure 8 are consistently below 0.04, indicating that both camera optical ports remained clear throughout the deployment, consistent with diver observation and post-recovery inspection. Variation in the camera metrics is primarily attributed to changes in the water quality during the deployment because flocculent or turbidity in the water close to the optical ports is illuminated by the LED backlight and increases the value of F, without actually fouling the port. Days with F value variations during the first 3 months of the deployment also have increased standard deviations, indicating that the variation is within the uncertainty of the measurement. During the last month of the deployment, the F values for Camera 1 (Cu, Wi, and CS) increase without an increase in the standard deviation, indicating a true change in the signal. Camera 1 (Cu, Wi, and CS) images are consistently brighter than those from Camera 2 (Cu and Wi) and have a larger range of variation. It is hypothesized that the light diffraction

FIGURE 7

Camera 1 (Cu, Wi, and CS) images of biofouling on the field testing frame from (a) March 19, (b) May 15, and (c) July 2 prior to recovery.

FIGURE 8

Averaged nightly biofouling metric values with shaded standard deviations on (a) Camera 1 (Cu, Wi, and CS) and (b) Camera 2 (Cu and Wi) optical ports throughout the endurance test.

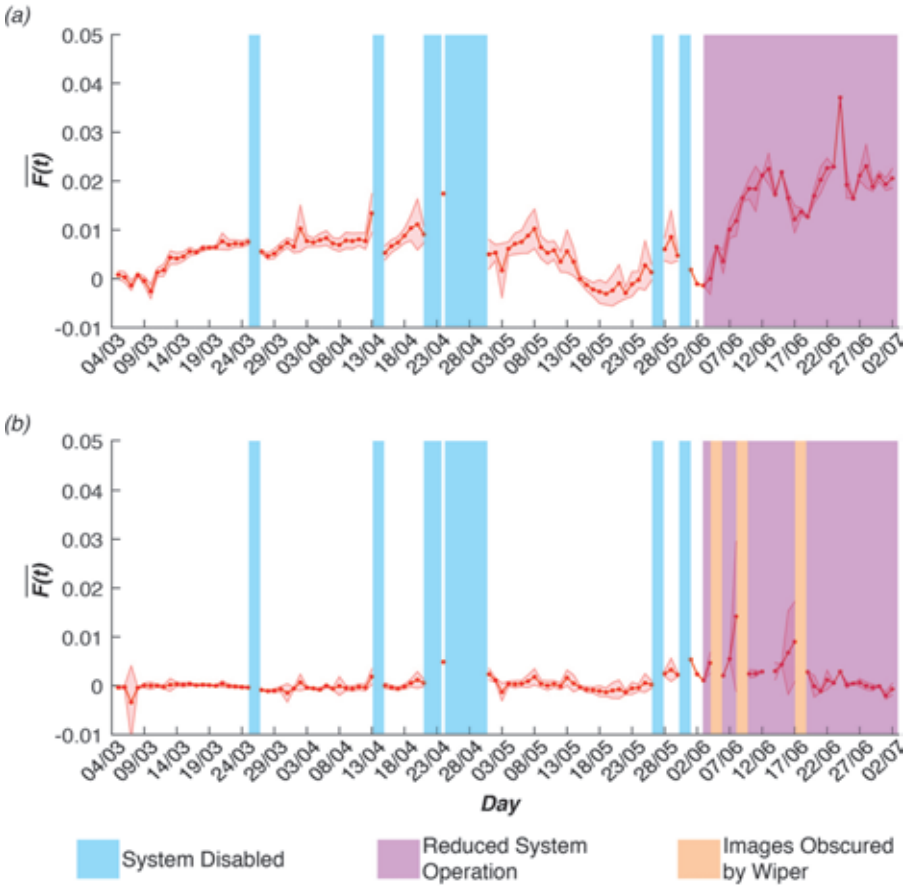

through the ClearSignal coating causes a "halo effect," increasing the number of bright pixels and magnifying any variation in brightness. Images obtained with external strobe illumination from the coated camera port are not of markedly lesser quality than the uncoated port, so this does not suggest that the coating degrades operational effectiveness. Counterintuitively, with the wipers activated only once per day at the end of the deployment, the fouling metric increases for Camera 1 (Cu, Wi, and CS), even though one would expect that the ClearSignal coating would mitigate fouling more effectively than the bare acrylic.

Post-recovery inspection of the system revealed severe macrofouling of every surface (including the back of the wiper blades) except for the camera optical ports. Figure 9 shows the center of the camera frame with a closeup view of the Camera 1 (Cu, Wi, and CS) optical port. Fouling on the system generally consisted of barnacles and algae and was independent of the surface orientation. The fouling release coating on Camera 1 (Cu, Wi, and CS) and Strobe 1 (Cu, Wi, and CS) optical ports was found to be slightly abraded (abrasion grooves in the arc of the wipers). The degradation of the coating, while not apparent in review of images acquired with strobe illumination, may have contributed to the fouling metric increase on Camera 1 (Cu, Wi, and CS) when illuminated by LED backlighting. As the wiper abraded the coating, the diffraction of light through the coating may have changed, or the surface may have become more susceptible to microfouling, both of which could contribute to an increase in the fouling metric for Camera 1 (Cu, Wi, and CS) over time.

FIGURE 9

Post-recovery biofouling on aluminum frame and camera optical ports.

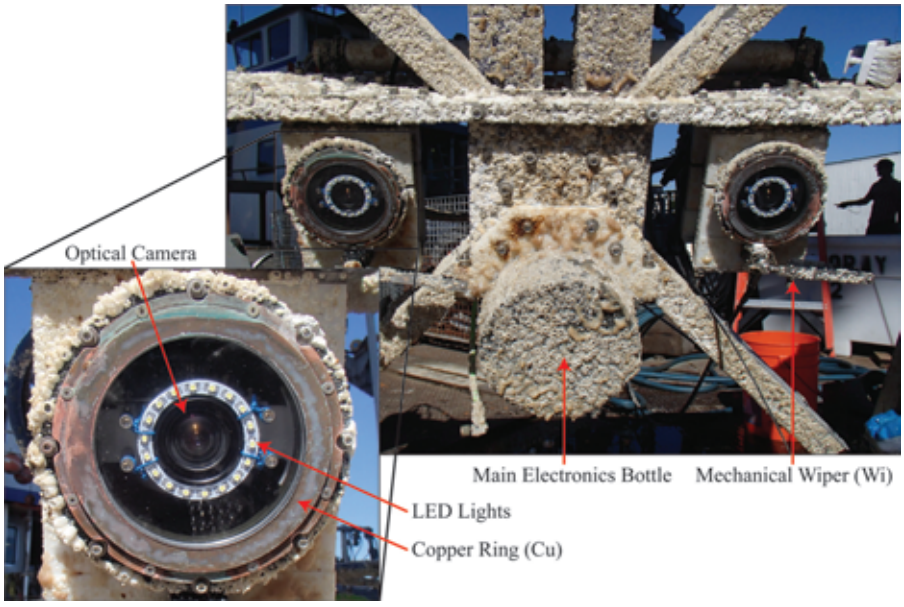

FIGURE 10

Biofouling on strobe optical ports with (a) Strobe 1 (Cu, Wi, and CS; though wiper rotated out of plane during test and was not effective for unknown period), (b) Strobe 2 (Cu and Wi), (c) Strobe 4 (Cu and Wi), and (d) Strobe 3 (Cu with six wiper actuations). Ordering identical to treatment schematic in Figure 4.

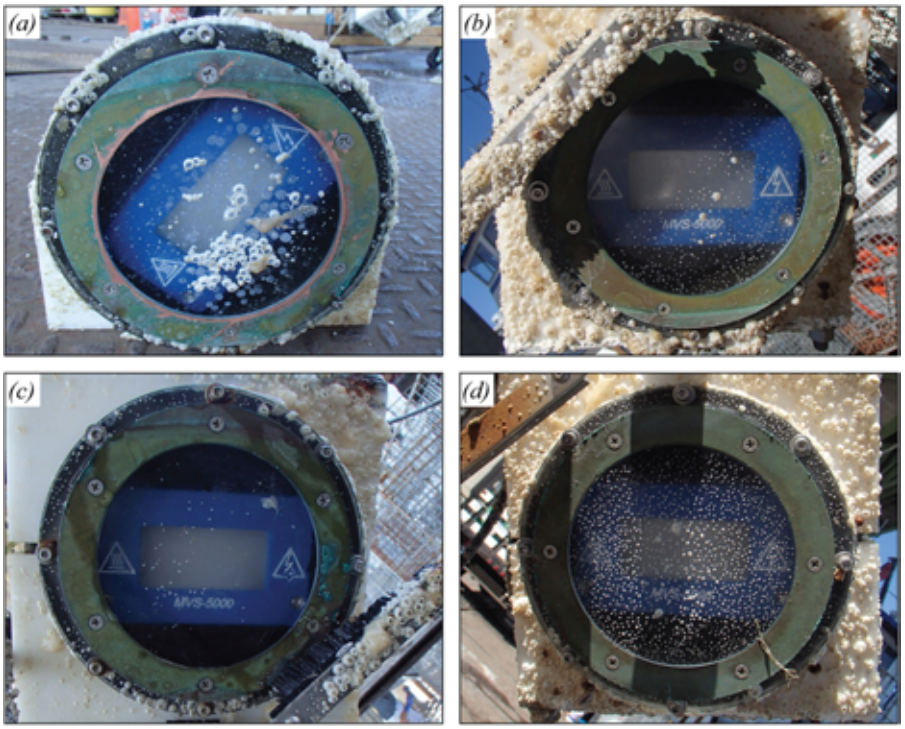

The strobe optical ports, which were not monitored during the deployment, other than qualitatively for the presence of fouling by the diver inspections, are shown after recovery in Figure 10. Due to the wipers being disabled over the last month of the deployment for the strobes (whereas the camera wipers were still actuated once each night), all four optical ports exhibit some barnacle growth. Strobe 1 (Cu, Wi, and CS) exhibits the most growth, though upon recovery, the wiper blade for this bottle was noted to have rotated out of the plane of the optical port, thus making it ineffective for a longer portion of the test than the wipers on the other strobe ports. Coincidentally, the Strobe 1 (Cu, Wi, and CS) optical port is also coated with ClearSignal, suggesting that the passive fouling mitigation measures (Cu and CS) would not be sufficient for multi-month deployments in adverse fouling conditions. Qualitative comparison of the camera and strobe optical ports demonstrates the effectiveness of the mechanical wiper to mitigate fouling (Figures 9 and 10).

Discussion and Conclusions

There are expected to be strong seasonal and spatial variations in biofouling within a region the size of Puget Sound (Dickey & Chang, 2001). The dates of this field deployment were chosen to span the spring and summer seasons, during which fouling is most severe. Since the endurance trial took place in calm waters with the camera system entirely within the photic zone, the biofouling observed during the trial was likely to be more severe than would occur at the anticipated deployment depth of 50 m.

Monitoring biofouling levels on camera optical ports in a quantitative manner is complicated by the variable nature of the imagery. This method of backlighting the optical ports with LEDs in the absence of external illumination provides a means to quantify temporal changes in the optical port clarity. While there was no apparent degradation in image quality during the deployment, the biofouling metric was able to detect more subtle changes than the human eye. An upward trend in this metric could, therefore, be used to predict the need for system maintenance before the optical port is visibly degraded, thus affording more time to plan system recovery (essential in marine renewable energy environments) and reducing system downtime.

The combination of mechanical and passive biofouling mitigation methods effectively prevented macrofouling growth that would have otherwise degraded system performance. The clarity of the camera optical ports in comparison to adjacent surfaces, as shown in Figure 9, is intuitively representative of this effectiveness. With no discernible difference between the clarity of the two camera optical ports, the benefit of the ClearSignal coating was minimal under the test conditions. The abrasion of the coating by the wiper brush suggests that the combination of these two antifouling measures is potentially detrimental with a wiper actuation frequency shorter than an hour. If a system deployment were to be power constrained, and the wipers could not be run as frequently (as would be the case for an autonomous

deployment), then a transparent coating may be helpful to maintain optical port clarity.

Separating the antifouling contributions of the copper rings from the wipers is difficult due to the lack of a true control. However, evaluation of the surfaces on the outside of the copper rings, which were not in contact with the wipers, suggests that the copper rings directly reduce fouling within a proximity of several millimeters. Similarly, for the optical port on Strobe 3 (Cu), which had fewer wiper activations, the most severe biofouling was at the center of the optical port, furthest from the copper ring. One hypothesis is that the presence of the ring contributed to this pattern, but without further testing, it is not possible to distinguish causality from correlation.

While the mechanical wipers play an important role in biofouling mitigation, they are only effective if they do not fail themselves. Integrating the wiper mount into the camera pressure vessel to control the interference spacing between the wiper and optical port would reduce the chance of wiper failures. For the prototype system described here, the spacing was set by hand prior to deployment, which may have resulted in inconsistent interference and caused the wiper malfunctions. The modular design of the Zebra-Tech Hydrowiper allows for easy integration, but caution should be taken to ensure proper and secure alignment. These modifications have been incorporated into the camera system design for the next iteration in system development (Joslin et al., 2014b; Rush et al., 2014).

For future deployments, measuring turbidity independently from the cameras and overlaying the measurement with the biofouling metric may allow correlations to be identified. This should be possible during subsequent system deployments, since the overall monitoring package can support additional instrumentation for an optical turbidity measurement. Biofouling of this turbidity measurement must be considered similarly to the cameras to avoid confounding the results.

The clarity of images obtained during this endurance trial suggests that optical camera deployments of at least 4 months are possible even under adverse fouling conditions with these biofouling mitigation measures. The results for these biofouling mitigation measures are consistent with the results for copper shuttered systems described in Manov et al. (2004), which have been shown to be effective for multi-month deployments. While the mechanical wiper does not protect the optical port by covering it between cycles like the shutter, it does not have to be activated every time data are acquired. The cleaning effect of the brush may also be greater than non-contact shuttered systems. While this result is most applicable to optical monitoring in Puget Sound, projects elsewhere involving long-term deployments of optical cameras may benefit from similar biofouling mitigation measures. Future deployments of this camera system for environmental monitoring of tidal energy projects will provide additional information about seasonal effectiveness of the measures employed.

Acknowledgments

The authors would like to thank Jeffery Thomas for use of his facilities at Sunset Bay Marina, Jim Thomson for coordination of the field deployment and inspection dives, Sandra Parker-Stetter and Sharon Kramer for recommendations on system testing, Capt. Andy Reay-Ellers for captaining the *R/V Jack Robertson*, Alex DeKlerk for designing and fabricating the imaging frame, Joe Talbert and Tim McGinnis for building the shore cable umbilical, Keith van Thiel for the design of the pressure housings and optical ports, Rick Towler and Kresimir Williams for insight into component selection and stereographic calibration, and last but certainly not least, Randy Sindelar for his adaptable custom electronics for power and communication.

Author Information:

James Joslin and Brian Polagye
Northwest National Marine
Renewable Energy Center
University of Washington,
Box 352600, Seattle, WA 98195-2600
Email: jbjoslin@u.washginton.edu;
bpolagye@u.washington.edu

References

ASTM D6990-05. 2011. Standard practice for evaluating biofouling resistance and physical performance of marine coating systems. West Conshohoken, PA, USA: ASTM International. http://dx.doi.org/10.1520/D6990-05R11.

Chave, A.D., Arrott, M., Farcas, C., & Farcas, E. 2009. Cyberinfrastructure for the US ocean observatories initiative: Enabling interactive observation in the ocean. In: Proceedings of MTS/IEEE Oceans 2009 – Europe. Bremen, Germany: MTS/IEEE.

Debiemme-Chouvy, C., Hua, U., Hui, F., Duval, J.L., Festy, D., & Cachet, H. 2011. Electrochemical treatments using tin oxide anode to prevent biofouling. Electrochem Acta. 56(28):10364-70. http://dx.doi.org/10.1016/j.electacta.2011.03.025.

Delauney, L., Compere, C., & Lehaitre, M. 2010. Biofouling protection for marine environmental sensors. Ocean Sci. 6(2):503-11. http://dx.doi.org/10.5194/os-6-503-2010.

Dickey, T.D., & Chang, G.C. 2001. Recent advances and future visions: Temporal variability of optical and bio-optical properties of the ocean. Oceanography. 14(3):15-29. http://dx.doi.org/10.5670/oceanog.2001.21.

Dobretsov, S., Williams, D.N., & Thomason, J. 2014. Biofouling methods. Oxford, UK: John Wiley & Sons, Ltd. http://dx.doi.org/10.1002/9781118336144.

Howe, B., & McGinnis, T. 2004. Sensor networks for cabled ocean observatories. In: International Symposium on Underwater Technology. UT: IEEE. pp. 113-20. http://dx.doi.org/10.1109/UT.2004.1405499.

Joslin, J., Celkis, E., Roper, C., Stewart, A., & Polagye, B. 2013. Development of an adaptable monitoring package for marine renewable energy. In: Proceedings of the MTS/IEEE Oceans 2013 Conference. San Diego, CA: MTS/IEEE.

Joslin, J., Polagye, B., & Parker-Stetter, S. 2014a. Development of a hybrid optical-acoustical camera system for monitoring tidal turbines. J Appl Remote Sens. 8:083633-1-25. http://dx.doi.org/10.1117/1.JRS.8.083633.

Joslin, J., Polagye, B., Rush, B., & Stewart, A. 2014b. Development of an adaptable monitoring package for marine renewable energy projects: Part II. Hydrodynamic performance. In: Proceedings of the 2nd Marine Energy Technology Symposium. Seattle, WA: Global Marine Renewable Energy Conference.

Manov, D.V., Chang, G.C., & Dickey, T.D. 2004. Methods for reducing biofouling on moored optical sensors. J Atmos Ocean Tech. 21:958-68. http://dx.doi.org/10.1175/1520-0426(2004)021<0958:MFRBOM>2.0.CO;2.

Phang, I.Y., Aldred, N., Clare, A.S., & Vancso, G.J. 2007. Effective marine antifouling coatings: Studying barnacle cyprid adhesion with atomic force microscopy. Nano. 1:36-41.

Polagye, B., Copping, A., Suryan, R., Brown-Saracino, J., & Smith, C. 2014. Instrumentation for monitoring around marine renewable energy converters: Workshop final report. Pacific Northwest National Laboratory, Seattle, WA. Tech. Rep. PNNL-23110.

Rush, B., Joslin, J., Stewart, A., & Polagye, B. 2014. Development of an adaptable monitoring package for marine renewable energy projects Part I: Conceptual design and operation. In: Proceedings of the 2nd Marine Energy Technology Symposium. Seattle, WA: Global Marine Renewable Energy Conference.

Salta, M., Wharton, J.A., Blache, Y., Stokes, K.R., & Briand, J.F. 2013. Marine biofilms on artificial surfaces: structure and dynamics. Environ Microbiol. 15(11):2879-93.

Whelan, A., & Regan, F. 2006. Antifouling strategies for marine and riverine sensors. J Environ Monitor. 8(9):880-6. http://dx.doi.org/10.1039/b603289c.

Woodroffe, A.M., Pridie, S.W., & Druce, G. 2008. The Neptune Canada junction box—Interfacing science instruments to sub-sea cabled observatories. In: Proceedings of MTS/IEEE Kobe Techno-Ocean. Kobe, Japan: MTS/IEEE.